www.lajss.org
Latin American Journal of Solids and Structures 6 (2009) 13–33

Comparison of journal orbits under hydrodynamic lubrication regime for traditional and Newton-Euler loads in combustion engines

André F. Carbonara, Durval Duarte Jr. and Marco L. Bittencourt

Department of Mechanical Design, Faculty of Mechanical Engineering, State University of Campinas, P.O. Box 6122, Zip Code 13083-970, Campinas, SP – Brazil

Abstract

When a force is applied on a hydrodynamic journal bearing of combustion engines under operating conditions, the journal axis moves with relation to the bearing center. This displacement can be determined by the eccentricity factor ϵ and the attitude angle α. Initially, it is necessary to calculate the dynamic forces that act on the bearing during actual operation. Based on the force and the bearing characteristics, it is then possible to design and implement a mathematical algorithm that calculates the journal orbit as a function of the crank angle. The algorithm is based on the solution of an algebraic system of force equilibrium under transient state. The hydrodynamic force at each time step is obtained by the solution of the Reynolds equation via the Finite Element Method. This paper analyzes the journal orbit of combustion engine bearings using the Newton-Euler and the traditional pseudo-dynamics approaches for the load calculation.

Keywords: Hydrodynamic lubrication, sliding bearings, Finite Element Method, combustion engine, dynamics, Reynolds equation

1 Introduction

The constant search for the improvement and increase in the market share of the automotive industry has stimulated the development of internal combustion engines with better performance, efficiency and lower price. In order to achieve these goals mathematical simulation has been a very important tool and used nowadays by most engine manufacturers.

The design of sliding bearings is also following this trend not only for the automotive industry but also for other areas of engineering. Several studies about bearings and hydrodynamic lubrication have been developed over last years both with mathematical simulation and experimental techniques. The mathematical simulation of bearings supply reliable data about the critical points of lubrication, cavitation and wear which in turn can be used to improve the final product.

In order to simulate the behavior of a hydrodynamic journal bearing under actual operating conditions, it is first necessary to have the loads as a function of the crank angle. In transient

*Corresp. author email: mlb@fem.unicamp.br Received 11 July 2008; In revised form 21 Oct 2008

analysis, these loads can be obtained from the calculation of the dynamic forces acting on the engine. This paper will discuss the effect of two different methods to calculate the dynamic forces in combustion engines.

A hypothesis usually used in the hydrodynamic simulation is to consider that the bearings, connecting rods and crank shaft are rigid. The combined study of hydrodynamic effects with the elastic deformation of the involved parts is known as Elasto-Hydrodynamic Lubrication (EHL) and have been studied by Wang [17], Fridman et al. [5], Stefani [16] and Garnier [6]. Models that take into account the effect of temperature variation have also been considered. Thermo-Hydrodynamic Lubrication (THL) models include the solution of the total energy equation and calculate the oil temperature as a function of time and position, which in turns alters significantly the lubricant oil viscosity (see Wang [19] and Zengeya [20]). More recently the combined effect of temperature and elastic deformation have been studied, mainly due to the rapidly increase in the computer processing power. Several papers about Thermo-Elasto-Hydrodynamic Lubrication (TEHL) models have been published as Kucinschi [11], Okamoto [14] and Fatu [3]. All of these papers show that the difference between the results of the simplest and the more complex models can be significative.

The hydrodynamic force can be obtained by the solution of the Reynolds equation with the Finite Elements Method (FEM). The application of one, two or three dimensional elements for the energy equation depends on the desired accuracy and computer processing time available. Wang [18] and Lehtovaara [12] present results that could be helpful for that choice.

Bukovnik et al. [2] studied several mathematical models of sliding bearings under transient state load in order to compare the accuracy of their results and computational time. The analyzes were performed for different engines, bearing and oil conservation conditions. The applied loads were calculated by the AVL EXCITE program [1].

Even though the classical Hydrodynamic Lubrication has been used with success in automotive applications, in other applications such as aerospace and nuclear engineering, bearings submitted to high velocities work with turbulent fluid flow and non negligible inertial forces. Frênea [4] studied this type of lubrication and concluded that these characteristics are relevant and in such areas it may be highly convenient to include these effects. Inertia effects were also studied by Nassab [13].

As it can be seen from this brief literature review, there are several ways for the mathematical modeling of hydrodynamic journal bearings, several numerical and analytical methods, different hypotheses about lubricants and some constructive bearing variables. Almost all of these variables have been studied intensively.

The objective of this paper is to study the effect of the load applied to the bearing under actual operating conditions. Specifically, the paper aims to compare two different theories used for the calculation of the dynamic loads in an automotive engine in what concerns the behavior of its bearings. Historically the most commonly used method is the so called Traditional Method [1]. There is another possibility which is based on the Rigid Body Dynamics and the Newton-Euler method [15]. Both types of loads are used as input data in a program that calculates the bearing

operating parameters and the results are then compared for a four stroke engine.

The paper is organized as follows. The first part deals with the dynamic loading calculation methods in a reciprocating engine. The main input data in the program is the load. In a conventional reciprocating engine, the acting forces on its internal elements (piston, connecting rod, crankshaft and bearings) are function of time due to its continuous geometrical alterations. The second part deals with the hydrodynamic lubrication theory needed to calculate the hydrodynamic forces that are generated by a bearing. The hydrodynamic lubrication theory allows the calculation of the acting forces on the bearing journal generated by the reaction of the pressurized oil film. This calculation is based on the Finite Element Method. The third part uses the results of the first two parts to construct an algebraic system of equations that represents the equilibrium of forces on the bearing which will supply the necessary variables to draw the bearing journal orbit. Finally, an example is considered to compare the orbit for the two types of loads.

2 Load Calculation

A complete cycle of a four stroke internal combustion engine corresponds to 720 degrees of crankshaft revolution. Each angular position corresponds to a particular geometrical configuration of the crankshaft-conrod-piston assembly. Another parameter that changes with the crank angle is the thermodynamic pressure over the piston which changes value at each cycle stage (admission, compression, explosion and exhaust). Due to these two factors, the distribution of forces between all the parts of this system is constantly altered throughout the 720 degrees of crankshaft revolution. This in turn alters the forces that act on the pins and bearings.

These forces have been calculated by the traditional method that makes use of simplifying hypotheses for the inertia force [9]. An alternative way to calculate the forces is through the Newton-Euler method which is based on the Rigid Body Dynamics and makes use of a systematic and considerably more consistent approach to represent the inertia and reaction forces.

Both methods were implemented in Matlab. The input data for the routines are the characteristics of the engine under analysis and also a curve that describes the pressure inside the cylinder as a function of the crank angle. It calculates all the forces acting on the engine throughout the 720 degrees of crankshaft along the whole cycle. These forces are utilized as input data for the simulation of the engine bearings under actual operating conditions.

2.1 Traditional Method

In the traditional modeling, the kinematics of the piston-conrod-crankshaft assembly is based on the geometric relationship of the pins associated to binomial series. Based on that, it is possible to determine the velocity and acceleration of the piston. After the deduction of the kinematics, the dynamics of the mechanism can be obtained. In this case, the inertial force is decomposed as a sum of rotating and oscillatory components. The equations presented below were obtained

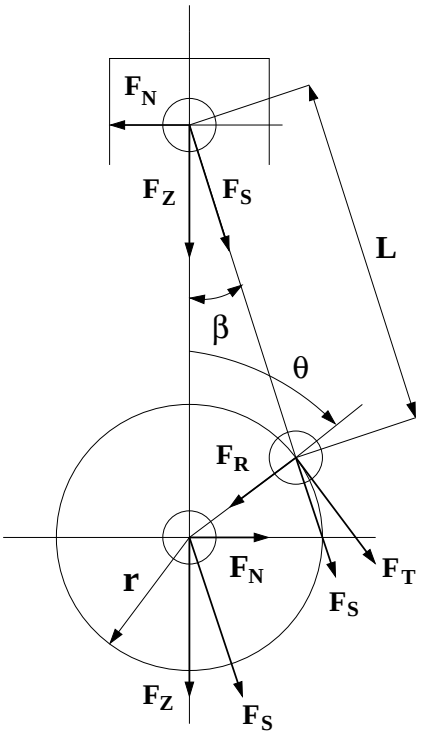

Figure 1: Geometrical and dynamic schemes for the traditional method [1].

from [1, 9].

The piston instantaneous position can be described as a function of the angles of Figure 1. Making use of trigonometric relations, it is then possible to find the position vector and its derivatives. From Figure 1, the instantaneous position of the piston is [1]

$$x = r\left(1 - \cos\theta\right) + L\left(\frac{\lambda}{2}\right)^2\left(1 - \cos 2\theta\right), \tag{1}$$

where $\lambda = \frac{r}{L}$, r is the crank radius and L is the conrod length. From the previous expression, the velocity and acceleration of the piston are respectively

$$v = \dot{x} = \dot{\theta} r\left(\sin\theta + \frac{\lambda}{2}\sin 2\theta\right), \tag{2}$$

$$a = \ddot{x} = \dot{\theta}^2 r\left(\cos\theta + \lambda\cos 2\theta\right). \tag{3}$$

In this approach, the inertia force is decomposed in its oscillatory and rotational components. For that purpose, the oscillation mass is defined usually as $m_o = \frac{1}{3}m_2 + m_3$ where m_2 and m_3 are the conrod and piston masses respectively. Analogously, the rotational mass is given by $m_r = \frac{2}{3}m_2$. More precisely for automotive engines, the following ranges of values are used

for the oscillatory and rotational masses $m_o = (0.2, 0.35)m_2 + m_3$ and $m_r = (0.65, 0.8)m_2$, respectively.

The alternating or oscillatory force is given as [1]

$$F_o = m_o\dot{\theta}^2 r\left(\cos\theta + \lambda\cos 2\theta\right). \tag{4}$$

The resulting force on the piston is

$$F_z = F_e - F_o, \tag{5}$$

where F_e is the gas force. The rotational component of the inertial force is defined as

$$F_r = m_r\dot{\theta}^2 r. \tag{6}$$

The tangential and radial forces acting on the crankshaft are calculated, respectively, as

$$F_T = F_z\frac{\sin\left(\theta+\beta\right)}{\cos\beta}, \tag{7}$$

$$F_R = F_z\frac{\cos\left(\theta+\beta\right)}{\cos\beta}. \tag{8}$$

The normal force on the cylinder can be determined by the following expression

$$F_N = F_z\tan\beta. \tag{9}$$

Finally, the resultant force on the connecting rod is

$$F_S = \frac{F_z}{\cos\beta}. \tag{10}$$

2.2 Newton-Euler Method

Initially, the kinematics of the piston-conrod-crankshaft system, illustrated in Figure 2, is obtained. After that the Newton-Euler equations are applied in order to determine the dynamic reactions [15].

The inertial reference system $I\left(X, Y\right)$ is at the center O of the crankshaft. Two moving reference systems are used. System $B_1\left(X_1, Y_1\right)$ rotates with the crankshaft and system $B_2\left(X_2, Y_2\right)$ moves with the conrod and the respective origins are at points O and B. The main system angles are denoted by θ and β, respectively, as indicated in Figure 2. The relation between them is given by

$$\beta = \arcsin\left(\frac{r}{L}\sin\theta\right) = \arcsin\left(\lambda\sin\theta\right). \tag{11}$$

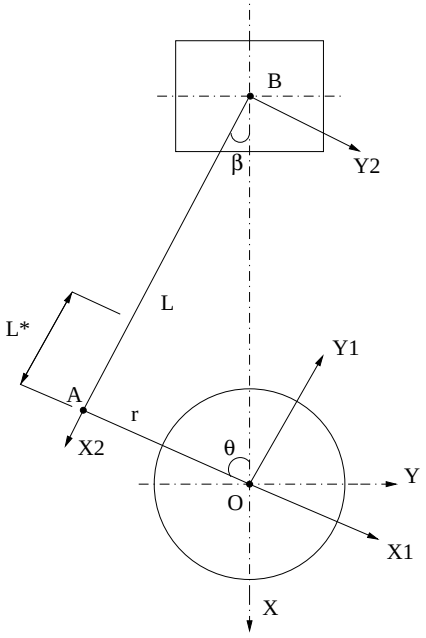

Figure 2: Piston-conrod-crankshaft mechanism.

The transformation matrices between the inertial and moving coordinate systems B_1 and B_2 are given, respectively, by

$$T_\theta = \begin{bmatrix} \cos\theta & \sin\theta & 0 \\ -\sin\theta & \cos\theta & 0 \\ 0 & 0 & 1 \end{bmatrix} \text{ and } T_\beta = \begin{bmatrix} \cos\beta & -\sin\beta & 0 \\ \sin\beta & \cos\beta & 0 \\ 0 & 0 & 1 \end{bmatrix} \tag{12}$$

The angular velocities of the moving bases B_1 and B_2 are respectively

$${}_{B_1}\vec{\Omega}_1 = \left\{ \begin{array}{ccc} 0 & 0 & \dot{\theta} \end{array} \right\}^T \text{ and } {}_{B_2}\vec{\Omega}_2 = \left\{ \begin{array}{ccc} 0 & 0 & -\dot{\beta} \end{array} \right\}^T. \tag{13}$$

The velocity of point A in the inertial basis can be determined from the following expression [15]

$${}_I\vec{v}_A = {}_I\,\vec{v}_O + {}_I\,\vec{\Omega}_1 \times {}_I\,\vec{r}_{OA} + {}_I\,\vec{v}_{rel}. \tag{14}$$

Using the basis B_1, the same velocity can be written as

$${}_I\vec{v}_A = {}_I\,\vec{v}_O + {}_I\,\vec{\Omega}_1 \times T_\theta^T\,{}_{B_1}\vec{r}_{OA} + T_\theta^T \frac{d}{dt}\left({}_{B_1}\vec{r}_{OA}\right), \tag{15}$$

where $\vec{v}_O = \vec{0}$ is the velocity of the point O. The position vector $\vec{r}_{OA}$, expressed in the basis B_1, is given by ${}_{B_1}\vec{r}_{OA} = \left\{ \begin{array}{ccc} -r & 0 & 0 \end{array} \right\}^T$. As $\vec{r}_{OA}$ is constant, the last term of the above equation is also zero. Therefore, the velocity of A in the inertial system reduces to

$${}_I\vec{v}_A = {}_I\,\vec{\Omega}_1 \times T_\theta^T\,{}_{B_1}\vec{r}_{OA} = \left\{ \begin{array}{ccc} \left(\dot{\theta} r \sin\theta\right) & \left(-\dot{\theta} r \cos\theta\right) & 0 \end{array} \right\}^T. \tag{16}$$

In a similar way, the velocity of point A can be written with the aid of the basis B_2 as

$$ {}_I\vec{v}_A = {}_I\,\vec{v}_B + {}_I\,\vec{\Omega}_2 \times T_\beta^T\, {}_{B_2}\vec{r}_{BA} + T_\beta^T \frac{d}{dt}\left({}_{B_2}\vec{r}_{BA}\right), \tag{17} $$

where ${}_{B_2}\vec{r}_{BA} = \left\{ \begin{array}{ccc} L & 0 & 0 \end{array} \right\}^T$ and ${}_I\vec{v}_B = \left\{ \begin{array}{ccc} v_B & 0 & 0 \end{array} \right\}^T$ is the piston velocity which is an unknown to be determined. Therefore,

$$ {}_I\vec{v}_A = {}_I\,\vec{v}_B + {}_I\,\vec{\Omega}_2 \times T_\beta^T\, {}_{B_2}\vec{r}_{BA} = \left\{ \begin{array}{ccc} \left(-\dot{\beta}L\sin\beta + v_B\right) & \left(-\dot{\beta}L\cos\beta\right) & 0 \end{array} \right\}^T. \tag{18} $$

Equating the velocities of point A obtained above with the aid of the bases B_1 and B_2, the following system of equations is obtained

$$ \left\{ \begin{array}{lcl} r\dot{\theta}\sin\theta & = & v_B - L\dot{\beta}\sin\beta \\ r\dot{\theta}\cos\theta & = & L\dot{\beta}\cos\beta \end{array} \right. . \tag{19} $$

From the above system, the following expressions for the conrod angular velocity $\dot{\beta}$ and the linear piston velocity v_B are determined and given, respectively, as

$$ v_B = \frac{r\dot{\theta}\sin\left(\theta+\beta\right)}{\cos\beta}, \tag{20} $$

$$ \dot{\beta} = \frac{r\dot{\theta}\cos\theta}{L\cos\beta}. \tag{21} $$

If the crankshaft rotates with constant angular speed, then the angular accelerations of the moving bases B_1 and B_2 are given respectively by ${}_{B_1}\dot{\vec{\Omega}}_1 = \left\{ \begin{array}{ccc} 0 & 0 & 0 \end{array} \right\}^T$ and ${}_{B_2}\dot{\vec{\Omega}}_2 = \left\{ \begin{array}{ccc} 0 & 0 & -\ddot{\beta} \end{array} \right\}^T$. The linear acceleration of point A can be described in the inertial basis as [15]

$$ {}_I\vec{a}_A = {}_I\,\vec{a}_O + {}_I\,\dot{\vec{\Omega}}_1 \times_I \vec{r}_{OA} + {}_I\,\vec{\Omega}_1 \times \left({}_I\vec{\Omega}_1 \times_I \vec{r}_{OA}\right) + 2{}_I\vec{\Omega}_1 \times_I \vec{v}_{rel} + {}_I\,\vec{a_{rel}}. \tag{22} $$

In a similar way to the velocity case, the acceleration of point A can be written with the aid of basis B_1 and

$$ \begin{array}{rcl} {}_I\vec{a}_A & = & {}_I\vec{a}_O + {}_I\,\dot{\vec{\Omega}}_1 \times T_\theta^T\, {}_{B_1}\vec{r}_{OA} + {}_I\,\vec{\Omega}_1 \times \left({}_I\vec{\Omega}_1 \times T_\theta^T\, {}_{B_1}\vec{r}_{OA}\right) \\ & + & 2{}_I\vec{\Omega}_1 \times T_\theta^T \frac{d}{dt}\left({}_{B_1}\vec{r}_{OA}\right) + T_\theta^T \frac{d^2}{dt^2}\left({}_{B_1}\vec{r}_{OA}\right). \end{array} \tag{23} $$

Since the bodies involved are rigid, the relative velocity and acceleration are zero. Consequently, the last two terms of the above equation are also zero. Therefore, equation (23) simplifies to

$$ {}_I\vec{a}_A = {}_I\,\vec{\Omega}_1 \times \left({}_I\vec{\Omega}_1 \times T_\theta^T\, {}_{B_1}\vec{r}_{OA}\right) = \left\{ \begin{array}{ccc} \left(r\dot{\theta}^2\cos\theta\right) & \left(r\dot{\theta}^2\sin\theta\right) & 0 \end{array} \right\}^T. \tag{24} $$

The acceleration of point A written in the basis B_2 is

$$\begin{aligned} {}_I\vec{a}_A &= {}_I\vec{a}_B + {}_I\dot{\vec{\Omega}}_2 \times T_\beta^T\, {}_{B_2}\vec{r}_{BA} + {}_I\vec{\Omega}_2 \times \left({}_I\vec{\Omega}_2 \times T_\beta^T\, {}_{B_2}\vec{r}_{BA}\right) \\ &+ 2{}_I\vec{\Omega}_2 \times T_\beta^T \frac{d}{dt}\left({}_{B_2}\vec{r}_{BA}\right) + T_\beta^T \frac{d^2}{dt^2}\left({}_{B_2}\vec{r}_{BA}\right). \end{aligned} \tag{25}$$

Again, the relative velocity and acceleration are zero and the above equation simplifies to

$${}_I\vec{a}_A = {}_I\,\vec{a}_B + {}_I\dot{\vec{\Omega}}_2 \times T_\beta^T\, {}_{B_2}\vec{r}_{BA} + {}_I\,\vec{\Omega}_2 \times \left({}_I\vec{\Omega}_2 \times T_\beta^T\, {}_{B_2}\vec{r}_{BA}\right), \tag{26}$$

where ${}_I\vec{a}_B = \left\{ \begin{array}{ccc} a_B & 0 & 0 \end{array} \right\}^T$ is the unknown piston acceleration. Therefore,

$${}_I\vec{a}_A = \left\{ \begin{array}{ccc} \left(a_B - L\ddot{\beta}\sin\beta - L\dot{\beta}^2\cos\beta\right) & \left(-L\ddot{\beta}\cos\beta + L\dot{\beta}^2\sin\beta\right) & 0 \end{array} \right\}^T. \tag{27}$$

Equating the accelerations of point A expressed in the bases B_1 and B_2, the following system of equations is obtained

$$\left\{ \begin{array}{lcl} r\dot{\theta}^2\cos\theta &=& a_B - L\ddot{\beta}\sin\beta - L\dot{\beta}^2\cos\beta \\ r\dot{\theta}^2\sin\theta &=& -L\ddot{\beta}\cos\beta + L\dot{\beta}^2\sin\beta \end{array} \right. . \tag{28}$$

The expression for the conrod angular acceleration $\ddot{\beta}$ and the piston linear acceleration a_B can be found by solving the above system. Therefore,

$$\ddot{\beta} = \frac{L\dot{\beta}^2\sin\beta - r\dot{\theta}^2\sin\theta}{L\cos\beta} = \dot{\beta}^2\tan\beta - \lambda\dot{\theta}^2\frac{\sin\theta}{\cos\beta}, \tag{29}$$

$$a_B = \frac{L\dot{\beta}^2 + r\dot{\theta}^2\cos\left(\theta+\beta\right)}{\cos\beta}. \tag{30}$$

The acceleration ${}_I\vec{a}_2^*$ of the conrod mass center can be written with the help of the basis B_2 as

$$\begin{aligned} {}_I\vec{a}_2^* &= {}_I\vec{a}_B + {}_I\dot{\vec{\Omega}}_2 \times T_{\beta B_2}\vec{r}_2^* + {}_I\,\vec{\Omega}_2 \times \left({}_I\vec{\Omega}_2 \times T_{\beta B_2}\vec{r}_2^*\right) \\ &+ 2{}_I\vec{\Omega}_2 \times T_\beta \frac{d}{dt}\left({}_{B_2}\vec{r}_2{}^*\right) + T_\beta \frac{d^2}{dt^2}\left({}_{B_2}\vec{r}_2{}^*\right), \end{aligned} \tag{31}$$

where ${}_{B_2}\vec{r}_2{}^* = \left\{ \begin{array}{ccc} L_{MC} & 0 & 0 \end{array} \right\}^T$ is the conrod mass center position vector on the basis B_2. According to Figure 2, $L_{MC} = L - L^*$. Taking into account the fact that the last two terms in equation (31) are zero, it is then possible to determine the acceleration of the conrod mass center as

$${}_I\vec{a}_2{}^* = \left\{ \begin{array}{ccc} \left(a_B - L_{MC}\ddot{\beta}\sin\beta - L_{MC}\dot{\beta}^2\cos\beta\right) & \left(-L_{MC}\ddot{\beta}\cos\beta + L_{MC}\dot{\beta}^2\sin\beta\right) & 0 \end{array} \right\}^T. \tag{32}$$

After the determination of the kinematics, it is then possible to apply the Newton-Euler equations to obtain the dynamic reactions in the connection pins of the mechanism. A detailed development is considered here just for the conrod which is modeled as a rigid body. The analysis of the crankshaft and piston are similar, but the piston is modeled as a particle.

Figure 3 illustrates the conrod free body diagram, including its weight (P_2) and the reactions in the small (F_{3x}, F_{3y}) and big (F_{2x}, F_{2y}) ends.

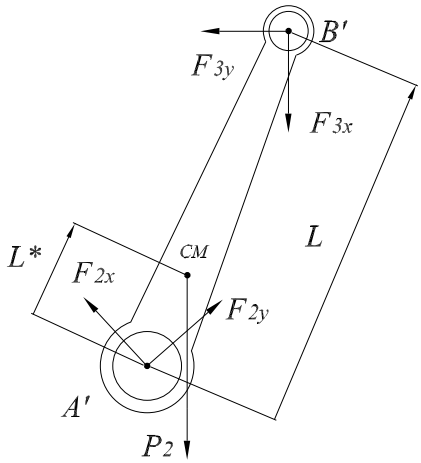

Figure 3: Conrod free body diagram. Forces (F_{2x}, F_{2y}) are represented in the B_2 reference system.

Applying Newton's second law with the force vectors represented in the inertial basis, the following equilibrium equation is obtained

$$ {}_I\vec{P}_2 + {}_I\,\vec{F}_2 + {}_I\,\vec{F}_3 = m_{2I}\vec{a}_2^{\,*}, \tag{33} $$

where ${}_I\vec{P}_2 = \left\{ \begin{array}{ccc} m_2 g & 0 & 0 \end{array} \right\}^T$ is the conrod weight; ${}_I\vec{F}_2 = \left\{ \begin{array}{ccc} F_{2x} & F_{2y} & 0 \end{array} \right\}^T$ and ${}_I\vec{F}_3 = \left\{ \begin{array}{ccc} F_{3x} & F_{3y} & 0 \end{array} \right\}^T$ are the reactions on the big and small bearing ends; and $\vec{a}_2^{\,*}$ is the the acceleration of the conrod mass center given in (32). Substituting these vectors in the previous expression results

$$ \left\{ \begin{array}{c} m_2 g \\ 0 \\ 0 \end{array} \right\} + \left\{ \begin{array}{c} -F_{2x} \\ -F_{2y} \\ 0 \end{array} \right\} + \left\{ \begin{array}{c} F_{3x} \\ F_{3y} \\ 0 \end{array} \right\} = m_2 \left\{ \begin{array}{c} a_B - L_{MC}\ddot{\beta}\sin\beta - L_{MC}\dot{\beta}^2\cos\beta \\ -L_{MC}\ddot{\beta}\cos\beta + L_{MC}\dot{\beta}^2\sin\beta \\ 0 \end{array} \right\}. \tag{34} $$

Considering the sum of moments with relation to the conrod mass center, the Euler equation can be written as [15]

$$ \sum_{i=1}^{n} {}_{B_2}\vec{M}_{MC_2} \quad = \quad {}_{B_2}I_{MC_2}\frac{d}{dt}({}_{B_2}\vec{\omega}_2) + {}_{B_2}\,\vec{\Omega}_2 \times ({}_{B_2}I_{MC_2\,B_2}\vec{\omega}_2) $$

$$+ \quad m_{2\,B_2}\vec{\rho}^{\,*}_{MC_2} \times_{B_2} \vec{a}_{MC_2}, \tag{35}$$

where ${}_{B_2}\vec{\omega}_2$ is the conrod angular velocity (in this case, it is equal to the angular velocity of the basis B_2, ${}_{B_2}\vec{\Omega}_2$); I_{MC_2} is the body inertia tensor with relation to the conrod mass center; ${}_{B_2}\vec{\rho}^{\,*}_{MC_2}$ is the distance between the conrod mass center and the point where the resultant of moments is considered and in this case ${}_{B_2}\vec{\rho}^{\,*}_{MC_2} = \vec{0}$. As the inertia tensor is calculated in the basis B_2, and assuming that the conrod is a symmetric body, the inertia tensor ${}_{B_1}I_{MC_2}$ is constant and diagonal. Therefore,

$${}_{B_2}I_{MC_2} = \begin{bmatrix} I_{xx_2} & 0 & 0 \\ 0 & I_{yy_2} & 0 \\ 0 & 0 & I_{zz_2} \end{bmatrix}. \tag{36}$$

Denoting ${}_{B_2}\vec{r}_{MC_{2A}} = \left\{ \begin{array}{ccc} L^* & 0 & 0 \end{array} \right\}^T$ as the position vector from the conrod mass center to the big end and ${}_{B_2}\vec{r}_{MC_{2B}} = \left\{ \begin{array}{ccc} -(L-L^*) & 0 & 0 \end{array} \right\}^T$ as the position vector from the conrod mass center to the small end, Euler equation reduces to

$${}_{B_2}\vec{r}_{MC_{2A}} \times T_\beta \left({}_I\vec{F}_2 \right) + {}_{B_2}\vec{r}_{MC_{2B}} \times T_\beta \left({}_I\vec{F}_3 \right) = {}_{B_2} I_{CM_2\,B_2}\dot{\vec{\Omega}}_2. \tag{37}$$

Developing the indicated operations, the following equilibrium equation is achieved

$$L^* \left(F_{2x}\sin\beta + F_{2y}\cos\beta\right) + \left(L - L^*\right)\left(F_{3x}\sin\beta + F_{3y}\cos\beta\right) = I_{zz_2}\ddot{\beta}. \tag{38}$$

The free-body diagram for the crankshaft is showed in Figure 4. Considering the crankshaft as a circular body (e.g., $\vec{r}^{\,*} = \vec{0}$), the equilibrium equations of forces and moment for the crankshaft are given, respectively, by [15]

$$\left\{ \begin{array}{c} m_1 g \\ 0 \\ 0 \end{array} \right\} + \left\{ \begin{array}{c} F_{1x} \\ F_{1y} \\ 0 \end{array} \right\} + \left\{ \begin{array}{c} F_{2x} \\ F_{2y} \\ 0 \end{array} \right\} = \left\{ \begin{array}{c} 0 \\ 0 \\ 0 \end{array} \right\}, \tag{39}$$

$$r\left(F_{1x}\sin\theta - F_{1y}\cos\theta\right) + M_{1z} = 0, \tag{40}$$

where (F_{1x}, F_{1y}) are the components of the reaction force on the main bearing and M_{1z} is the torque.

Figure 5 illustrates the piston free body diagram which is modeled as a particle. The equilibrium equation for the piston is given by

$$\left\{ \begin{array}{c} m_3 g \\ 0 \\ 0 \end{array} \right\} + \left\{ \begin{array}{c} 0 \\ N \\ 0 \end{array} \right\} + \left\{ \begin{array}{c} -F_{3x} \\ -F_{3y} \\ 0 \end{array} \right\} + \left\{ \begin{array}{c} F_e \\ 0 \\ 0 \end{array} \right\} = m_3 \left\{ \begin{array}{c} a_B \\ 0 \\ 0 \end{array} \right\}, \tag{41}$$

where (F_{3x}, F_{3y}) are the components of the reaction force on the small bearing end and N is the normal force between the piston and cylinder wall.

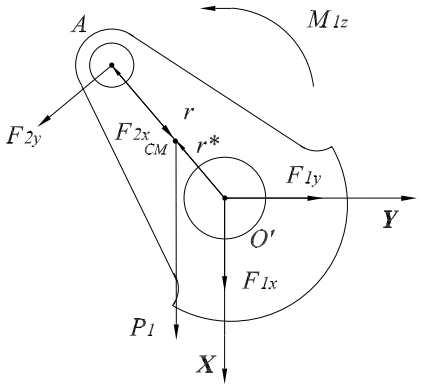

Figure 4: Crankshaft free body diagram.

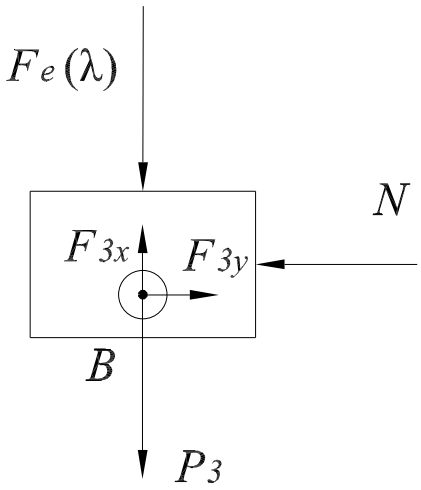

Figure 5: Piston free body diagram.

The equilibrium equations (34), (38), (39), (40) and (41) can be written as a system of algebraic equations whose unknown are the dynamic reactions. This system is solved for each point of the applied pressure curve generating the load throughout the 720 degrees of the engine cycle.

3 Solution of the Reynolds Equation

The solution of the Reynolds equation determines the pressure field and the hydrodynamic force generated by the bearing. This force is compared to the applied load in order to reach the equilibrium or orbital point. This work assumes rigid bearing behavior and uses the Reynolds boundary conditions. Basically, the Reynolds equation is obtained from the Navier-Stokes equations assuming a thin oil film with negligible curvature of the Newtonian fluid in laminar flow [8]. For a dynamic load, the Reynolds equation is [18,19]

$$\frac{1}{r_J^2}\frac{\partial}{\partial\theta}\left(h^3\frac{\partial P}{\partial\theta}\right)+\frac{\partial}{\partial z}\left(h^3\frac{\partial P}{\partial z}\right)=6\mu\Omega\frac{\partial h}{\partial\theta}+12\mu\frac{\partial h}{\partial t}, \tag{42}$$

where P is the pressure distribution, h is the oil thickness function, μ is the oil viscosity, Ω is the angular speed and r_J^2 is the bearing radius.

The weak form of the previous strong form is obtained multiplying equation (42) by a test function v and integrating on the domain. Therefore,

$$\int_\Omega\left(\frac{1}{r_J^2}\frac{\partial}{\partial\theta}\left(h^3\frac{\partial P}{\partial\theta}\right)+\frac{\partial}{\partial z}\left(h^3\frac{\partial P}{\partial z}\right)\right)v d\Omega=\int_\Omega\left(6\mu\Omega\frac{\partial h}{\partial\theta}+12\mu\frac{\partial h}{\partial t}\right)v d\Omega. \tag{43}$$

After integration by parts, the previous equation becomes

$$\int_\Omega\left(\frac{h^3}{r_J^2}\frac{\partial P}{\partial\theta}\frac{\partial v}{\partial\theta}+h^3\frac{\partial P}{\partial z}\frac{\partial v}{\partial z}\right)v d\Omega=\int_\Omega\left(6\mu\Omega\frac{\partial h}{\partial\theta}+12\mu\frac{\partial h}{\partial t}\right)v d\Omega+\int_\Gamma\left(h^3\frac{\partial P}{\partial\theta}n_\theta+h^3\frac{\partial P}{\partial z}n_z\right)v d\Gamma, \tag{44}$$

where v is the test function and (n_θ, n_z) are the components of the normal vector on the boundary Γ of the domain Ω. Assuming that the pressure is zero along Γ, the boundary integral is also zero as v must satisfy the same homogeneous boundary condition.

Using a Galerkin approximation, the pressure distribution and the test function are approximated on each element of the mesh as

$$P(\theta,z)=\sum_{i=1}^{n}a_iN_i(\theta,z)\ \text{ and }\ v(\theta,z)=\sum_{j=1}^{n}b_jN_j(\theta,z), \tag{45}$$

where n is the number of nodes and $N_i(\theta,z)$ the elemental shape functions.

Substituting the previous expression in (44) and after simplifications, the element weak form of the Reynolds equation for $j=1,\ldots,n$ is given by

$$\sum_{i=1}^{n}\left(\int_{\Omega_e}\left(\frac{h^3}{r_J^2}\frac{\partial N_i}{\partial\theta}\frac{\partial N_j}{\partial\theta}+h^3\frac{\partial N_i}{\partial z}\frac{\partial N_j}{\partial z}\right)d\theta dz\right)a_i=\int_{\Omega_e}6\mu\Omega\frac{\partial h}{\partial\theta}N_j d\theta dz+\int_{\Omega_e}12\mu\frac{\partial h}{\partial t}N_j d\theta dz. \tag{46}$$

The left hand side represents the stiffness matrix and the right integral gives the dynamic force term. After the assembling of the element stiffness matrices and solution of the resulting system of equations, the pressure distribution on the bearing sliding surface is obtained. The integrals of the pressure distribution give the values of the hydrodynamic forces acting on the bearing journal [8]. One important point is to locate the θ-coordinate for the cavitation region, where the pressure becomes negative. The Reynolds procedure has been used in this work.

4 Determination of the Orbits

In this section, the method used to calculate the orbital points is considered. Other algorithms are presented in [7]. Figure 6 shows a radial hydrodynamic bearing. Points O and O' indicate the centers of the bearing and bearing journal, respectively. The eccentricity e is the distance between the centers O and O'. Here α is the attitude angle between the line of centers and the vertical axis Y.

The external load applied at time t is indicated by the vector $\mathbf{W_{XY}(t)}$ expressed by (see Figure 6)

$$\mathbf{W_{XY}(t)}=\left\{\begin{array}{c}W_x(t)\\W_y(t)\end{array}\right\}=\left\{\begin{array}{c}W\sin\phi(t)\\-W\cos\phi(t)\end{array}\right\}. \tag{47}$$

In order to determine the orbit of the journal center of a hydrodynamic bearing, it is necessary to calculate the eccentricity factor $\epsilon=\frac{e}{c}$ and the attitude angle α, where c is the journal bearing clearance.

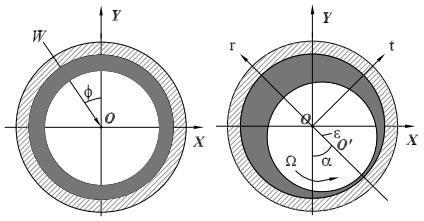

Figure 6: Radial hydrodynamic bearing.

Figure 6 also illustrates the cartesian XY and polar rt coordinate systems. It is possible to transform the load $\mathbf{W}$ from the system XY to the system rt in the following way

$$\mathbf{W}_{rt}=\left[\begin{array}{cc}-\sin\alpha & \cos\alpha\\ \cos\alpha & \sin\alpha\end{array}\right]\mathbf{W}_{XY}. \tag{48}$$

Therefore, from equations (47) and (48)

$$W_r(t)=-W_x(t)\sin\alpha(t)+W_y(t)\cos\alpha(t), \tag{49}$$

$$W_t(t)=W_x(t)\cos\alpha(t)+W_y(t)\sin\alpha(t). \tag{50}$$

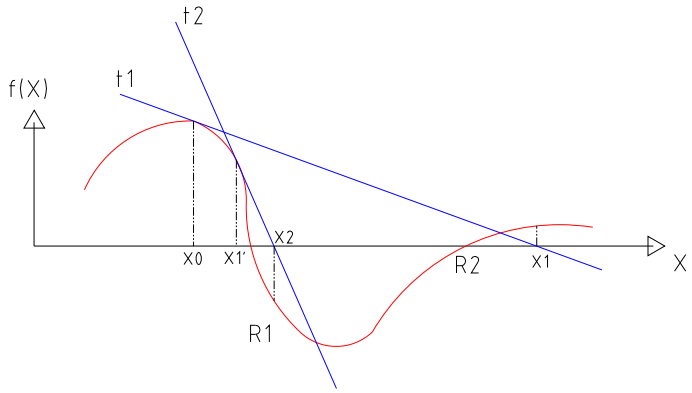

Figure 7: Sub-relaxation method.

The construction of the linear system considers the approximation of the hydrodynamic forces by first order Taylor series [10]. Based on the forces on the journal at time steps n and $n+1$ and the forces with relation to the unknowns ϵ and α, it is possible to determine the new coordinates that will provide the equilibrium of the forces. The hydrodynamic force in the following time step can be calculated by using the first term of the Taylor series

$$F_r{}^{n+1} = F_r^n + \frac{\partial F_r}{\partial \alpha}\Delta\alpha + \frac{\partial F_r}{\partial \epsilon}\Delta\epsilon, \tag{51}$$

$$F_t{}^{n+1} = F_r^n + \frac{\partial F_t}{\partial \alpha}\Delta\alpha + \frac{\partial F_t}{\partial \epsilon}\Delta\epsilon. \tag{52}$$

In the equilibrium, the hydrodynamic forces at the time level under consideration are equal to the applied loads. The equilibrium condition can be written in matrix notation as

$$\begin{bmatrix} \frac{\partial F_r}{\partial \alpha} & \frac{\partial F_r}{\partial \epsilon} \\ \frac{\partial F_t}{\partial \alpha} & \frac{\partial F_t}{\partial \epsilon} \end{bmatrix} \begin{bmatrix} \Delta\alpha \\ \Delta\epsilon \end{bmatrix} = \begin{bmatrix} -(W_r{}^{n+1} - F_r{}^n) \\ -(W_t{}^{n+1} - F_t{}^n) \end{bmatrix}. \tag{53}$$

The solution of this system of equations gives the variations of the independent variables which are added to the current position of the journal center. The convergence is reached only if a sub-relaxation factor is used, which is a multiplier $0 < \delta \leq 1$. Figure 7 illustrates how this method works. Assumes that the zero X_1 of the function's tangent at point X_0 approaches the zero of the function f. X_1 is closer to the root R_2 and the following iterations would lead to an incorrect root R_2. This phenomenon happens usually in systems which have roots very close to each other due to their extremely sensitivity and non-linear characteristics. Therefore, the algorithm may proceed based on a fraction X_1' of X_1 . It can be noticed now that the zero X_2 of the function's tangent at the point X_1' is close to root R_1, which leads to correct convergence in the following iterations. The factor δ increases at each iteration until the unitary value is achieved and consequently convergence is assured. The results presented in this paper were obtained using a sub-relaxation factor $\delta = \frac{n}{10}$ if $n <= 10$ and $\delta = 1$ if $n > 10$, where n is the iteration number. It can be seen that the factor becomes unitary after the 10th iteration.

The calculation of the derivatives of the hydrodynamic forces are based on [10]. Given a point on the orbit, small perturbations $\delta\epsilon$ and $\delta\alpha$ are added to the independent variables ϵ and α. The resulting

hydrodynamic forces due to these perturbations are then calculated. From there, the approximation of the derivatives of the forces with relation to the independent variables are given by

$$\frac{\partial F_r}{\partial \epsilon} \approx \frac{F_r\left(\epsilon+\delta\epsilon\right)-F_r(\epsilon)}{\delta\epsilon}, \tag{54}$$

$$\frac{\partial F_r}{\partial \alpha} \approx \frac{F_r(\alpha+\delta\alpha)-F_r(\alpha)}{\delta\alpha}, \tag{55}$$

$$\frac{\partial F_t}{\partial \epsilon} \approx \frac{F_t(\epsilon+\delta\epsilon)-F_t(\epsilon)}{\delta\epsilon}, \tag{56}$$

$$\frac{\partial F_t}{\partial \alpha} \approx \frac{F_t(\alpha+\delta\alpha)-F_t(\alpha)}{\delta\alpha}, \tag{57}$$

The values of $\delta\epsilon$ and $\delta\alpha$ were found by trial and error and case 5% of ϵ and α were used.

Two different convergence criteria are used: maximum difference between the applied and hydrodynamic loads and maximum variation of the independent variables between two consecutive iterations. The first criterium is used only if the second one is satisfied.

In order to verify the convergence of forces, the calculated values of $\Delta\epsilon$ and $\Delta\alpha$ are summed up to their initial values. Then the final values are used for the solution of the Reynolds equation. The resulting hydrodynamic force is compared to the input load using

$$\frac{\|\mathbf{F}_h-\mathbf{W}\|}{\|\mathbf{F}_h\|} \leq \delta_1. \tag{58}$$

The second convergence criterium is based on the difference in the independent variables at each iteration. Three variables are checked: the variation in the eccentricity factor ϵ, the angle α and the length of the arc drawn by two adjacent points in the journal orbit ($\epsilon\alpha$). Therefore,

$$|\alpha^{n+1}-\alpha^n| \leq \delta_2, \tag{59}$$

$$\left|\epsilon^{n+1}-\epsilon^n\right| \leq \delta_3, \tag{60}$$

$$\left|\epsilon^{n+1}\left(\alpha^{n+1}-\alpha^n\right)\right| \leq \delta_4. \tag{61}$$

The following values were used for the precisions δ_i aiming to balance the accuracy and the computing processing time: $\delta_1 = 1\times10^{-5}$, $\delta_2 = 5^o$, $\delta_3 = 0.05$ and $\delta_4 = 0.075$. If all the conditions are satisfied then the precision of the orbit point is warranted. This new point is given by the coordinates $(\epsilon+\Delta\epsilon,\alpha+\Delta\alpha)$. Repeating this process over the 720 degrees of crankshaft revolution, the full orbit of the bearing journal center is drawn. If convergence is not achieved, the time step is reduced until the converge criterium is achieved.

5 Results

Consider the following relevant dimensions of a four cycle Otto engine with four cylinders

- piston diameter: $d = 96.00mm$;
- piston stroke: $L_s = 102.50mm$;
- conrod length: $L = 175.44mm$;

- bearing radius: $r = 29.37mm$;
- bearing width: $b = 26.32mm$;
- bearing radial clearance: $c = 52.50\mu m$;
- oil viscosity: $\mu = 10.00mPas$;
- crankshaft segment mass: $m_1 = 0.56Kg$;
- conrod mass: $m_2 = 1.30Kg$;
- piston mass: $m_3 = 1.25Kg$;
- conrod inertia moment: $I_{zz_2} = 0.0034Kgm^2$;
- position of the conrod mass center: $L^* = 58.48mm$.

The range of angular speed is 1800 to 5400 RPM and 9 pressure curves were considered. The orbits of the conrod journal were obtained using the two load types discussed previously. The dynamic loads for the two approaches and the respective orbits are shown in Figures 8 to 16 for each pressure curve.

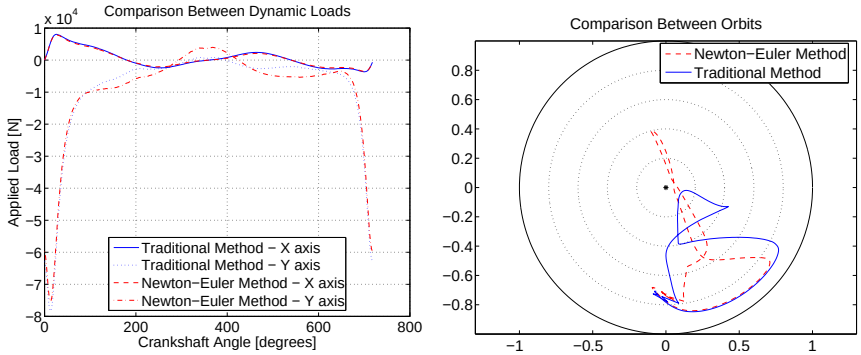

(a) Loads. (b) Orbits.

Figure 8: Load and orbit of conrod bearing journal at 1800 rpm.

The results in Figures 8 to 16 were calculated with pressure curves increasing with the rotational engine speed. The pressures peaks are around 110 MPa in lower speeds and reaches 140 MPa in higher speeds. Close to the explosion angle, the influence of the inertia forces are lower than the gas forces. In general, the Newton-Euler method provides greater inertia forces. Consequently, the dynamic reactions close to explosion are lower with Newton-Euler method. These less intense reactions lead to lower eccentricity factors in higher speeds, when Newton-Euler method is considered. It can be inferred that the traditional method results in overestimated eccentricity factors. Greater eccentricity factors are associated with higher oil pressure inside the bearing, and therefore, higher stresses. As the main factors in the design of bearings are pressure and stress, the Newton-Euler method is more recommended than the traditional approach.

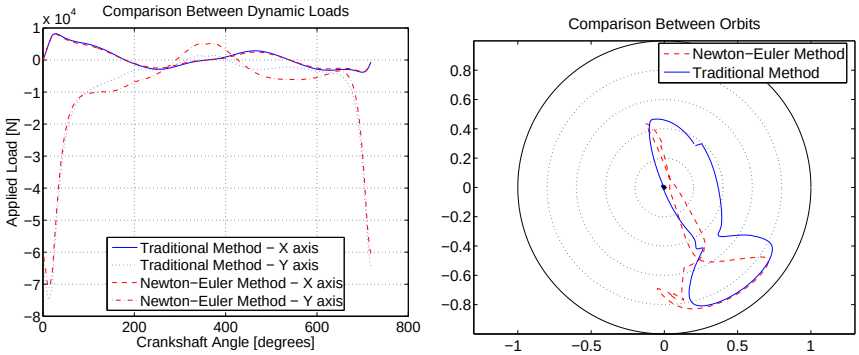

(a) Loads. (b) Orbits.

Figure 9: Load and orbit of conrod bearing journal at 2000 rpm.

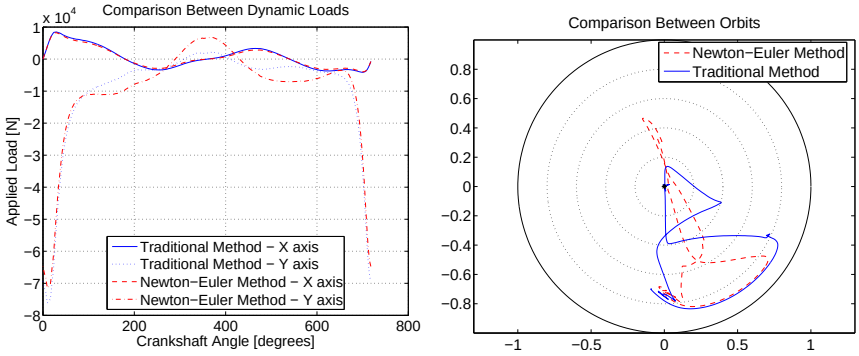

(a) Loads. (b) Orbits.

Figure 10: Load and orbit of conrod bearing journal at 2200 rpm.

6 Conclusions

This paper presented two methods to calculate the dynamic reactions on the pins of the piston-conrod-crankshaft mechanism of inline internal combustion engines. The first approach is the Traditional Method that has been commonly used in the automotive engineering. It is based on the decomposition of the inertia force in oscillatory and rotational components. The second approach is the Newton-Euler Method which is theoretically more consistent.

Results for a typical four-stroke, four-cylinder, Otto cycle engine showed that the inertia forces are super-estimated in the traditional approach. This is illustrated in Figure 17 for the traditional oscillatory inertia force and the Newton-Euler inertia force on the piston. The oscillatory mass of the traditional approach may be adjusted in such way that two approaches may become similar. But this become useless if the Newton-Euler approach is available. On the explosion region of the pressure curves, the two approaches are not very different as in this case the explosion forces are more important. Outside the explosion region, the inertia forces become important and the two methods show greater differences,

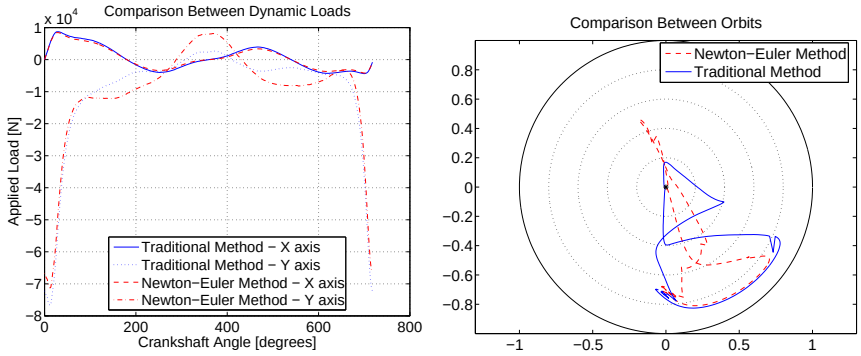

(a) Loads. (b) Orbits.

Figure 11: Load and orbit of conrod bearing journal at 2400 rpm.

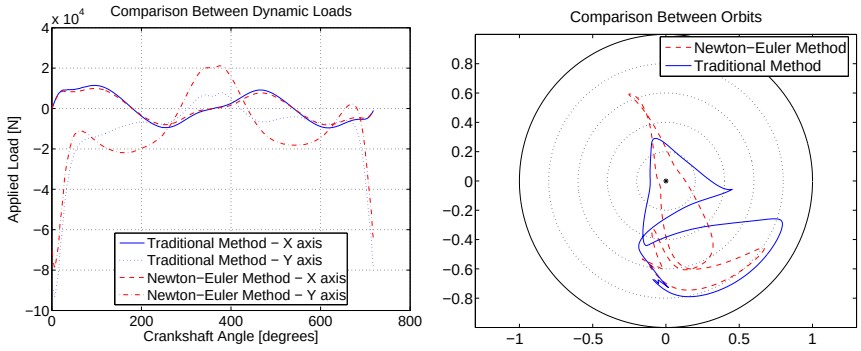

(a) Loads. (b) Orbits.

Figure 12: Load and orbit of conrod bearing journal at 3800 rpm.

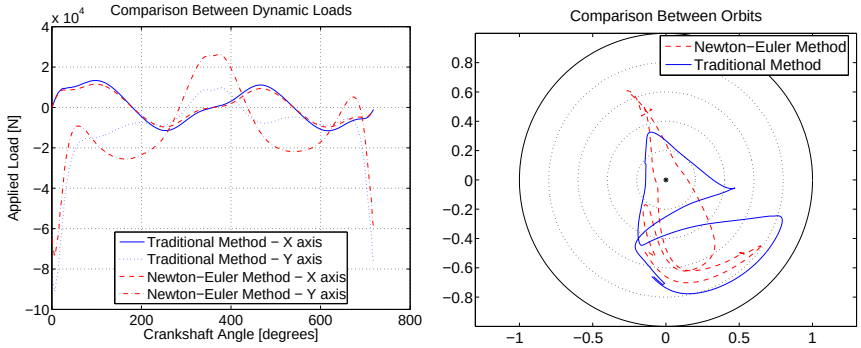

(a) Loads. (b) Orbits.

Figure 13: Load and orbit of conrod bearing journal at 4200 rpm.

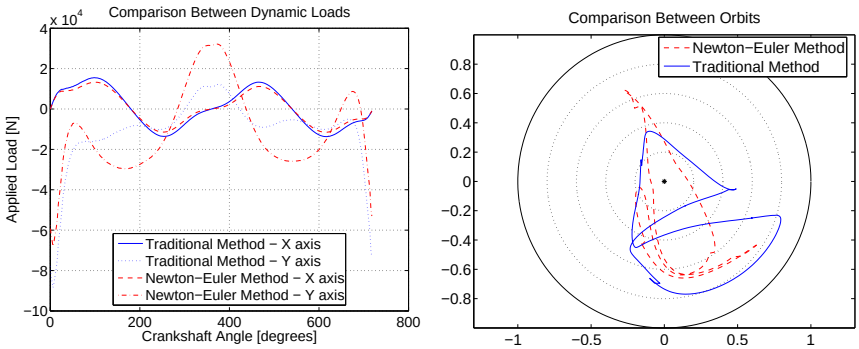

(a) Loads. (b) Orbits.

Figure 14: Load and orbit of conrod bearing journal at 4600 rpm.

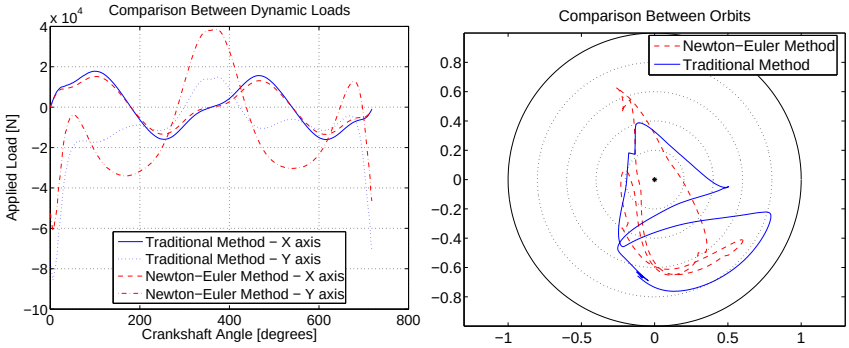

(a) Loads. (b) Orbits.

Figure 15: Load and orbit of conrod bearing journal at 5000 rpm.

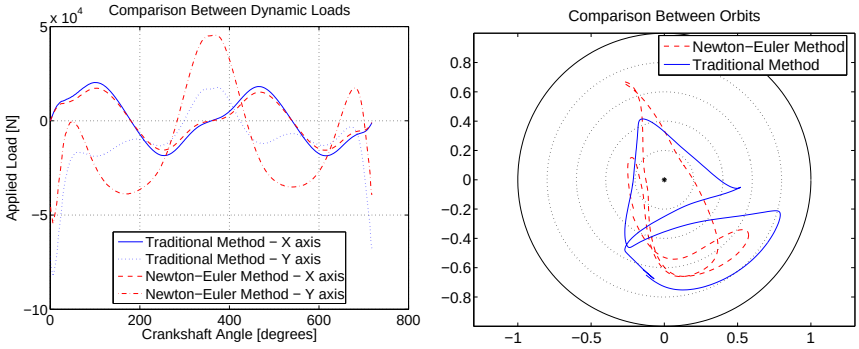

(a) Loads. (b) Orbits.

Figure 16: Load and orbit of conrod bearing journal at 5400 rpm.

mainly when the rotational speed is increased.

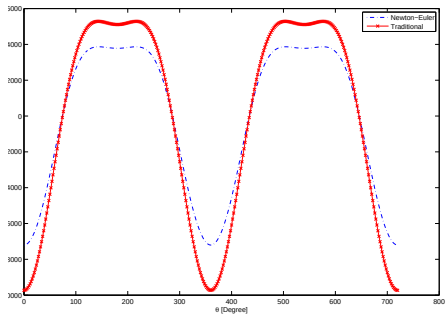

Figure 17: Inertia forces on the piston.

Higher pressures and stresses are to be expected in bearings when the traditional approach is used compared to the Newton-Euler Method.

References

[1] AVL. *AVL Excite Designer - Theory*, 2004.

[2] Sasa Bukovnik, Nicole Dorr, Valdas Caika, Wilfried J. Bartz, and Bernhard Loibnegger. Analysis of diverse simulation models for combustion engine journal bearings and the influence of oil condition. *Tribology International*, 39(8):820–826, 2006.

[3] A. Fatu, M. Hajjam, and D. Bonneau. A new model of thermoelastohydrodynamic lubrication in dynamically loaded journal bearings. *Journal of Tribology*, 128(1):85–95, 2006.

[4] Jean Frênea. Combined thin-film and Navier-Stokes analysis in high Reynolds number lubrication. *Tribology International*, 39(8):734–747, 2006.

[5] Vladimir M. Fridman, Ilya L. Piraner, and Carl F. Musolff. Some applications of the hydrodynamic and elasto-hydrodynamic analysis to the diesel engine bearings. In *Proceedings of the ASME/STLE International Joint Tribology Conference*, pages 807–829, Long Beach, CA, United States, 2004. ASME Tribology Division;Society of Tribologists and Lubrication Engineers, STLE, American Society of Mechanical Engineers.

[6] Thierry Garnier. Three-dimensional ehd behavior of the engine block/crankshaft assembly for a four cylinder inline automotive engine. *Journal of Tribology, Transactions of the ASME*, 121(4):721–730, 1999.

[7] P.K. Goenka. Dynamically loaded bearings: finite element method analysis. *Journal of Tribology*, 106:429–439, 1984.

[8] B.J. Hamrock, S.R. Schmidt, and B.O. Jacobson. *Fundamentals of Fluid Film Lubrication*. Marcel Dekker Inc., 2nd edition, 2004.

[9] J. B. Heywood. *Internal Combustion Engine Fundamentals*. McGraw-Hill, 1998.

[10] Durval Duarte Jr. *Tribology, Lubrification and Sliding Bearings (in portuguese)*. Editora Ciência Moderna, Brazil, Rio de Janeiro, 2005.

[11] B. Kucinschi. A transient thermoelastohydrodynamic study of steadily loaded plain journal bearings using finite element method analysis. *Journal of Tribology*, 122(1):219–226, 2000.

[12] Arto Lehtovaara. A numerical model for the calculation of transient hydrodynamic lubrication of journal bearings. *Tribologia - Finnish Journal of Tribology*, 25(1):23–30, 2006.

[13] S. A. Gandjalikhan Nassab. Inertia effect on the thermohydrodynamic characteristics of journal bearings. *Journal Proceedings of the Institution of Mechanical Engineers*, 219(6):459–467, 2005.

[14] Y. Okamoto. Numerical analysis of lubrication in a journal bearing by a thermoelastohydrodynamic lubrication (tehl) model. *International Journal of Engine Research*, 6(2):95–105, 2005.

[15] Ilmar Ferreira Santos. *Dynamics of Mechanical Systems (in portuguese)*. Makron Books, Brazil, São Paulo, 2001.

[16] Fabrizio A. Stefani and Alessandro U. Rebora. A nonlinear structure based elastohydrodynamic analysis method for connecting rod big end bearings of high performance engines. *Journal of Tribology*, 126(4):664–671, 2004.

[17] Daen Wang, Theo Keith, Qingmin Yang, and Vaidyanathan Kumar. Lubrication analysis of a connecting-rod bearing in a high-speed engine. Part ii: Lubrication performance evaluation for non-circular bearings. *Tribology Transactions*, 47(2):290–298, 2004.

[18] Li-Ping Wang. Weighted finite element method for computing nonlinear oil-film forces in journal bearing. *Engineering Mechanics*, 23(5):163–167,156, 2006.

[19] Xiaoli Wang. Thermo-hydrodynamic analysis of dynamically loaded bearings. *Journal of Tsinghua University*, 39(8):30–33, 1999.

[20] M. Zengeya, M. Gadala, and G. Segal. Three-dimensional modeling of thermohydrodynamic lubrication in slider bearings using streamline upwind Petrov-Galerkin method. *Numerical Heat Transfer. Part A: Aplications*, 49(10):947–968, 2006.